

PAPER • OPEN ACCESS

Wafer-scale fabrication of target arrays for stable generation of proton beams by laser-plasma interaction.

To cite this article: R L Zaffino *et al* 2018 *J. Phys.: Conf. Ser.* **1079** 012007

View the [article online](#) for updates and enhancements.



IOP | ebooks™

Bringing you innovative digital publishing with leading voices to create your essential collection of books in STEM research.

Start exploring the collection - download the first chapter of every title for free.

Wafer-scale fabrication of target arrays for stable generation of proton beams by laser-plasma interaction.

R L Zaffino¹, M Seimetz², A Ruiz³, I Sanchez³, P Mur², P Bellido², R Lera³, D Quirion¹, L Martín⁴, J Benlliure⁴, J M Benlloch², M Lozano¹ and G Pellegrini¹

¹Instituto de Microelectrónica de Barcelona IMB-CNM-CSIC 08193 Barcelona, Spain

²Instituto de Instrumentación para Imagen Molecular I3M-CSIC, Universitat Politècnica de València, Camino de Vera s/n, Ed. 8B-N-1^a, 46022 Valencia, Spain

³Proton Laser Applications S. L., Av. Vilafranca del Penedés 11a, 08734 Olérdola, Barcelona, Spain

⁴Dpto Física de Partículas, Campus Vida, USC, Rúa Xoaquín Días de Rábago S/N, 15782 Santiago de Compostela, Spain

rossella.zaffino@imb-cnm.csic.es

Abstract. Large-scale fabrication of targets for laser-driven acceleration of ion beams is a prerequisite to establish suitable applications, and to keep up with the challenge of increasing repetition rate of currently available high-power lasers. Here we present manufacturing and test results of large arrays of solid targets for TNSA laser-driven ion acceleration. By applying micro-electro-mechanical-system (MEMS) based methods allowing for parallel processing of thousands of targets on a single Si wafer, sub-micrometric, thin-layer metallic membranes were fabricated by combining photolithography, physical and chemical vapor deposition, selective etching, and Si micromachining. These structures were characterized by using optical and atomic force microscopy. Their performance for the production of laser-driven proton beams was tested on a purpose-made table-top Ti:Sapphire laser system running at 3 TW peak power with a contrast over ASE of 10^8 . We have performed several test series achieving maximum proton energy values around 2 MeV.

1. Introduction

In the next years a series of high power laser installations will be available worldwide with the ability of operating at repetition rates (1÷10 Hz) never before experienced. This working regime will require thousands of consumable targets per day to sustain experimental campaigns, so that it is extremely relevant to develop methods allowing for mass production and characterization of targets with high versatility for the different experimental needs [1]. In addition to production, target positioning, alignment, and refreshment are of the same importance for the proper target design of a given application. Targets for high-power laser experiments are of different densities ranging from gaseous to solid state, including foams and cryogenic materials. Here, we restrict our attention to solid state



targets for laser-driven proton acceleration through Target Normal Sheath Acceleration (TNSA) [2] which is the prevailing mechanism in the experiments conducted so far. Targets used for TNSA laser irradiation have been typically thin foils of metallic or dielectric materials with thicknesses up to tens of microns [3]. More recently, the improvement in laser contrast over ASE, and the advancement in material science technologies, allowed for exploring sub-micrometric thicknesses, with promising results with respect to the maximum proton energies. In this work, we made use of MEMS based manufacturing to fabricate thin membranes of conductive materials integrated in a Si wafer. These were used as targets for TNSA laser irradiation with a purpose-made 3 TW laser system. MEMS processing such as pattern transfer, material deposition and selective etching make it possible to achieve simple (2D) or complex (3D) target configurations, allowing for parallel manufacturing of thousands of targets with high reproducibility of specimen belonging to the same wafer, and between wafers of the same batch. For these reasons, and due to their availability on industrial scale developed by the semiconductor industry, they appear especially adequate for the technological developments expected within the field of high-power lasers.

2. Target fabrication and characterization.

A schematic of the process flow applied to obtain a single membrane is shown in Fig.1 joint with an example of the pattern transferred onto a standard p-type <100> silicon wafer, double side polished, with a thickness of 525 μm . The principal steps are: photolithography on wafer front side, followed by back side metallization, and metal etching. For some samples, we also added a back side photolithography used to reduce the metallic pattern corresponding to the window opened on the front wafer side.

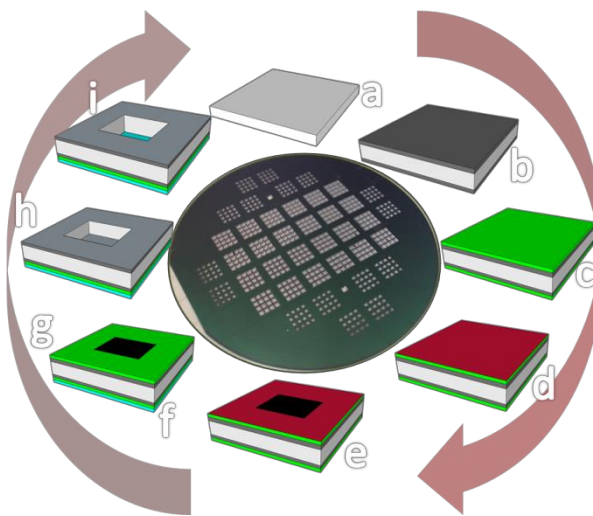


Figure 1. Schematic of the process flow for the fabrication of an individual membrane. In the centre an example of a 4 inch wafer with embedded membranes.

As first step Si wafers (Fig.1-a) were wet oxidized to grow either a 100 nm (at 950°C) or 400 nm thick (at 1100°C) SiO_2 layer, Fig. 1-b. This was followed by the deposition of a 180 nm thick low pressure chemical vapour deposition (LPCVD) layer of Si_3N_4 (Fig.1-c) on front side of the wafer corresponding to the laser entry side of the target. In the subsequent step, a 1.2 μm thick layer of the (positive) photoresist HIPR 6512 (Fig1-d) was spun on the same wafer side and exposed to UV light (using a Canon PLA600 mask aligner) through a photomask to define the area and the spatial distribution of the target membranes (Fig.1-e-f). Thereafter, etching of exposed $\text{Si}_3\text{N}_4/\text{SiO}_2$ layers was achieved by a dry process using a mixture of $\text{Ar}/\text{CHF}_3/\text{CHF}_4$ (in the Applied Material Precision 5000 Mark II P5

system). The remaining photoresist was stripped in a TePla 300-E plasma system (Technics Plasma, USA). Then, we processed the rear wafer side. First, the desired thickness of the membrane material (Fig.1-g), either Al or a tri-layer composed by Ti-Ni-Au, was sputtered using the Kenosistec KSH800 or the Material Research Corporation 903 equipment, employed respectively for aluminium and gold based metallization. Nickel and titanium, or a chromium layer, is standardly used to improve the intrinsic poor attachment of gold over SiO₂. Following back-side metallization, a 2 μm thick layer of photoresist AZ 6512 was spin-coated and exposed to UV light (not represented) using a Canon PLA600 mask aligner through a photomask allowing for patterning of the rear side of targets. The pattern is finally shaped by either wet etching of Al or of Ti-Ni-Au. The last step of the whole process is bulk Si micromachining (Fig.1-h) on the front wafer side necessary to open windows for the laser-interaction with the membranes. This is achieved by anisotropic etching in 40% KOH at 80°C during about 10 hours. The process relies on the fact that KOH has different etching rates on silicon crystal planes: it is fastest for (100) and (110) planes and lowest for (111) resulting in the characteristic “V” shaped 3D structures like truncated pyramids. Si micromachining is spontaneously stopped by the underlying buried oxide. To protect the metalized rear wafer side during Si micromachining a uniform layer of wax was deposited and baked during 1 h at 100°C. The wax dissolves easily in toluene and can be removed just before target delivery. Finally, for some samples we etched the underlying SiO₂ (Fig.1-i) by dip HF. Thin film thickness measurements were realized by using the Nanospec AFT 200 by Nanometrics for at least 5 different locations of each processed wafer; the final result is the average of these points. Optical microscopy characterization of membranes was accomplished by using the optical microscope by LEICA model DMLM. Analysis of surface roughness has been done with the atomic force microscopy by Veeco IV dimension, and scanning for each sample an area of 1 μm×1 μm. Aluminium membranes were fabricated having three thicknesses: 0.25 μm, 0.65 μm and 1 μm whereas in the case of gold based ones, we considered only two, 70 nm and 100 nm, which were both adhered over 20 nm titanium and 30 nm of nickel. For some cases, membranes were used tethered on the SiO₂, or the oxide layer was removed by dip HF. Each wafer located a total of 640 thin-layer membranes, out of which 384 have a surface area of 1 mm², and the remaining, of 0.5 mm². It is clear that the smaller the surface area, the greater will be the number of available targets for each wafer and consequently the lower will be the cost of each consumable membrane. Also, the robustness of submicrometric material layers is higher for reduced surfaces. However, this should be considered alongside the requirements for laser alignment and focusing, a part that for damage propagation at higher laser intensity than considered here. For this reason, we chose to fabricate two different area membranes and to analyse the implications on laser focusing which will be discussed in the following section. In general, it is important to remark that this is not ideal from the fabrication point of view because the etching time differs according to the structure size. For example, in our case we need to apply a supplementary etching time in order to complete Si micromachining of 0.25 mm² membranes, while keeping the others protected from the extra etching time which, at already opened windows, would result in breakage of metallic membranes. For each wafer, the fabrication yield was calculated as the difference between the numbers of intact membranes out of all target cells (Fig.2 (a) and (b)), resulting in an average of about 0.6 for all the productions (30 wafers). Normally, target fabrication is achieved in a place different from the laser installation and safe target transport should be also accounted as a further step of target production. We observed that keeping the wax layer on the metallized side and storing the wafers between the protective plastics which are thermally adhered for wafer dicing allow for a comfortable and safe target transport. Release of individual target cells could be finally realized at the laser installation. In this way, membranes fabricated according to the strategy presented are delivered in a format which is easy to manipulate inside the interaction chamber and adaptable to different experimental setups and needs, making it possible moreover to try several experimental conditions (thickness, material composition, local surface treatment) at once.

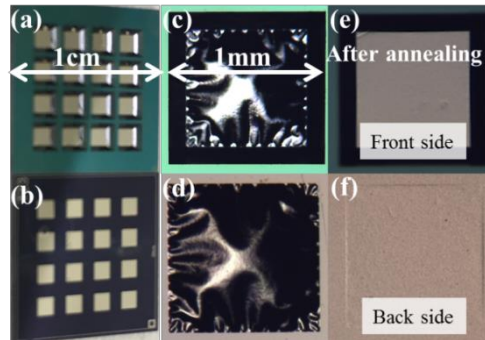


Figure 2. Back (a) and front (b) side of an individual target cell loading 16 membranes. Compressive stress shown by membranes following fabrication (c) and (d), and its release to tensile stress after annealing (e) and (f).

It is common to find that after fabrication, membranes exhibit compressive stress which is characterized by the presence of worm-like folding of the surface such as that in Fig. 2(c)-(d). The emergence of stress in membranes has been subject of much research in the field of CMOS technologies for the role they have in the correct functioning of many semiconductor based devices, and several methods for stress compensation have been proposed [5], [6]. In our case, surface folding could lead to difficulties for laser focusing and alignment, as well as for shot-to-shot reproducibility as we will discuss in the next section. For this reason, it is preferable to have membranes in a state of tensile stress causing material elongation so that their surfaces appear flat such that of Fig. 2(e)-(f). To achieve release of compressive stress into tensile one, we applied a short annealing at 400°C during 90 sec. which was found effective both for aluminium and gold based membranes. This could be done at the end of the fabrication right before using targets. We could observe that for free-standing membranes, i.e., that obtained after SiO₂ etching, compressive stress spontaneously releases after dip HF process. Thereafter, we characterized the membranes' surface roughness by using AFM which results are shown in Fig. 3. The picture shows the nanostructured character of the deposited film also referred as “cauliflower morphology” due to the fact that larger grains are formed by the aggregation of smaller ones. Grains size changes with film thickness.

Surface roughness is important for focus determination through the back reflection of visible laser light (speckle). In fact, in order to apply this method, as explained in [7], it is necessary that surface roughness be in the range of the laser wavelength. For all analysed samples we are far from reaching this value. For the thickest ones, which are expected to be also the roughest ones, we could only measure an average roughness of about 100 nm whereas for all remaining cases it stays in the range of a few nanometers. For this reason, in order to determine the focus position through the speckle we glued on top of each target cell a slice of aluminium foil allowing for clear visualization of the interference pattern. However, in order to account for the effects of inaccurate focus determination we mapped proton energy within a distance of $\pm 100 \mu\text{m}$ from the focus estimated initially.

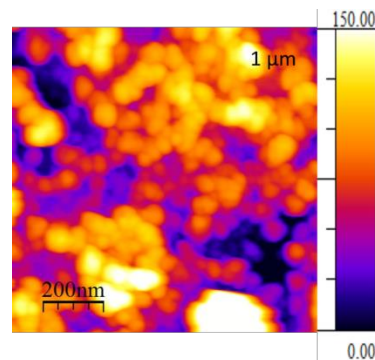


Figure 3. Roughness characterization of an aluminium membrane 1 μm thick through AFM.

3. Proton acceleration experiments

All experiments were conducted at a 3 TW/55 fs table-top laser system having 165 mJ pulse energy behind the compressor. It can operate both in single shot mode and up to 100 Hz repetition rate. The system is based on chirped pulsed amplification (CPA) and it has been developed specifically for laser-proton acceleration by one of the partners [4]. Following compression, laser pulses are injected into the interaction chamber kept at a pressure of about 10^{-2} mbar which is sufficient to prevent laser filamentation and deceleration of protons before reaching particle detectors. Laser pulses are then focused on the target by a $f/3$ gold coated off-axis parabolic mirror (OAP) at an incidence angle of 30° . A 632 nm He:Ne laser is coupled into the same optical path of the principal Ti:Sa beam and used to control the target positioning in transverse direction. Characterization of accelerated particles was achieved by means of CR-39 plates placed at 100 cm distance behind the target, and a time-of-flight (TOF) detector based on a fast plastic scintillator located at a distance of 237 cm from the target. Both detectors were calibrated with standard particle beams at the National Accelerator Centre (CNA) at Seville. Proton acceleration experiments were performed in single shot modality. Individual target alignment and focusing has been done for the first membrane of each target cell used. All data were taken with 1 mm^2 membranes. For a series of shots within the same target cell we assumed that the focus does not vary from one membrane to the subsequent ones and thus maintained a reference position. In order to study the dependency of the proton energies on the longitudinal position we moved away from the established focus in steps of $\pm 50 \mu\text{m}$. Thereafter, we obtained the maximum proton energy for aluminum and gold bases membranes of different thicknesses for both free-standing and SiO_2 tethered membranes. For each thickness, the maximum proton energy is calculated averaging over the highest values of energy measured in the focus position. The values obtained are coherent with previous results showing that with high contrast ($>10^8$) thinner targets are better energy converters [8]–[13]. An example of obtained results is shown in Fig. 4(a) for gold based membranes. This is the typical energy distribution around the focus position obtained for each analyzed thickness, independently from the material used. Although for many specimens a parabolic shape around the zero position has been observed, the corresponding energy variations within $\pm 50 \mu\text{m}$ account for only 10% of the value measured in the exact focus. This is interesting in view of the development of applications requiring high rate repetition operability. In fact, whereas at low frequency it is possible to perform even single target alignment, at high frequency this possibility is lost so that it is important that off-focus energy values suffer only slight variations. For both aluminum and gold based membranes, we could observe that data from free-standing and SiO_2 tethered membranes differ by 5-10% (Fig. 4(b)).

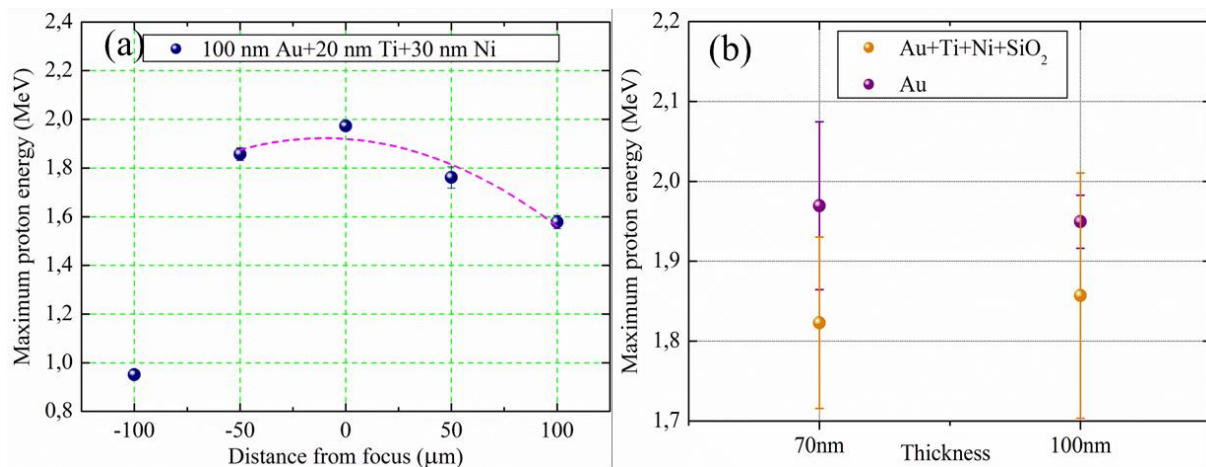


Figure 4. (a) Maximum proton energy distribution around focus position. (b) Comparison between maximum proton energy obtained with free-standing and SiO₂ tethered membranes.

The higher energy with pure Au may be intuitive because the membrane with oxide layer is significantly thicker. In addition, in our set-up, the laser pulse interacts first with the metallic, and then with the semiconductive layer which could prevent the effective propagation of the electric sheath inside the target. However, these findings deserve a deeper analysis with less parameter variability and a better contrast over ASE. The only observation we can affirm at present is that under current working conditions, the presence of the SiO₂ behind the metallic membrane is not especially relevant, while avoiding the dip HF etching of this layer can in general improve the yield of fabrication.

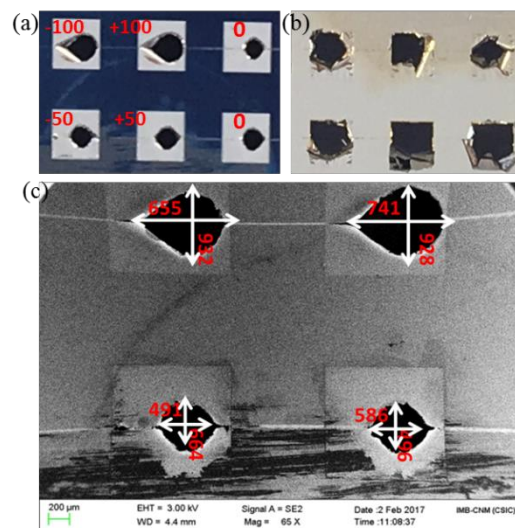


Figure 5. Comparison between shock propagation in (a) double side photolithography membranes and (b) all-metalized rear side membranes. (c) Astigmatism in tracks left by laser shots off-focus.

Another interesting remark arose from the post-shot target analysis between membranes belonging to target cells with photolithography also on the back wafer side (see Fig. 5 (a)) and bottom (Fig. 5 (b)). Although we could observe, as represented in Fig. 5 (b), that membranes after shots look more damaged when they belong to a double-side photolithography target cell. This phenomenon should be investigated at higher laser intensity, because it is well-known that target damage and “fratricide” are not an issue below 1 J. It is also interesting to observe that being completely destroyed after interaction, these membranes do not show tracks of the off-focus alignment chosen in some case to study proton energy dependence, which are on the other side appreciable on membranes of Fig. 5 (a).

The progressive off-focus introduced alters the shape of the hole left by laser which becomes more elliptical and tends to have a bigger area than in the case of membranes shot in the focus position. In general, laser damage propagates over an area which is two orders of magnitude bigger (Fig. 5 (c)) than the laser-spot area estimated to be $\approx 5.0 \times 11.5 \mu\text{m}^2$ (FWHM). The size of damage propagation is significant with respect to mask design because it limits from below the opening area available for laser interaction. This has also consequences for the array density one can consider which becomes relevant for high repetition rate operability.

Finally, we compared data obtained from MEMS based membranes with data recorded from plain foils of the same thickness and material (aluminum) from benchmark experiments conducted with the same laser system [4]. According to our results, the use of MEMS membranes improves the proton acceleration performance of a 30% (in case of $0.65 \mu\text{m}$ thick targets) and of a 9.8% (in case of $1 \mu\text{m}$ thick targets) [14]. Here too, further studies with higher statistics will be necessary to corroborate these findings.

4. Conclusions

We have presented the fabrication of submicrometric, conductive, thin-layer membranes embedded in a Si wafer according to a MEMS based manufacturing approach. This combines standard photolithography, material layer deposition, selective etching and bulk Si micromachining. Photolithography is used to rapidly pattern the Si surface in such a way to define windows on the front wafer side having the same area of metallic membranes deposited on the rear wafer side. Finally, Si micromachining allows for opening windows on the front side thus making membranes, either free-standing or tethered on a nanometric SiO_2 layer, accessible for laser interaction. Gold, and aluminum, based membranes were fabricated with variable thicknesses below $1 \mu\text{m}$ and were used as targets for laser-driven proton acceleration through the TNSA mechanism showing better efficiency in energy conversion compared to standard foil targets used for benchmark experiments at the same laser installation.

MEMS based manufacturing offers many advantages for target fabrication as compared to different methods which mainly rely on manual and individual target arrangements. Among these, the reproducibility of the fabrication thanks to parallel processing, the controllability of membrane thickness and composition over a wide range of options, and the possibility of target manufacturing over large area substrates by using conventional microfabrication facilities. Indeed, the degree of target complexity, for example, through the introduction of 3D surface modification could be straightforwardly considered. All these elements would foster the cheap fabrication of simple and even complex targets useful for high-power, high repetition rate lasers experiments and would contribute to the development of applications based on ultra-intense laser-plasma interactions.

Acknowledgements

This work has made use of the Spanish ICTS Network MICRONANOFABS partially supported by MEINCOM. This project has been financed by the Spanish Ministry for Economy and Competitiveness within the Retos- Colaboración 2015 initiative, ref. RTC-2015-3278-1. P. Mur has received a grant of the Garantía Juvenil 2015 program.

References

- [1] I. Prencipe, J. Fuchs, S. Pascarelli, D. W. Schumacher, R. B. Stephens, N. B. Alexander, R. Briggs, M. Büscher, M. O. Cernaianu, A. Choukourov, M. De Marco, A. Erbe, J. Fassbender, G. Fiquet, P. Fitzsimmons, C. Gheorghiu, J. Hund, L. G. Huang, M. Harmand, N. J. Hartley, A.

- Irman, T. Kluge, Z. Konopkova, S. Kraft, D. Kraus, V. Leca, D. Margarone, J. Metzkes, K. Nagai, W. Nazarov, P. Lutoslawski, D. Papp, M. Passoni, A. Pelka, J. P. Perin, J. Schulz, M. Smid, C. Spindloe, S. Steinke, R. Torchio, C. Vass, T. Wiste, R. Zaffino, K. Zeil, T. Tschentscher, U. Schramm, and T. E. Cowan, "Targets for high repetition rate laser facilities: needs, challenges and perspectives," *High Power Laser Sci. Eng.* 5, e17, 2017.
- [2] M. Roth and M. Schollmeier, "Ion Acceleration - Target Normal Sheath Acceleration," Proceedings of the CAS-CERN Accelerator School: PlasmaWake Acceleration, Geneva, Switzerland, <http://dx.doi.org/10.5170/CERN-2016-001.231>, 2017.
- [3] A. Macchi, M. Borghesi, and M. Passoni, "Ion acceleration by superintense laser-plasma interaction," *Rev. Mod. Phys.*, 85(2), 751 (43), 2013.
- [4] P. Bellido, R. Lera, M. Seimetz, A. Ruiz-De La Cruz, S. Torres-Peirò, M. Galán, P. Mur, I. Sánchez, R. Zaffino, L. Vidal, A. Soriano, S. Sánchez, F. Sánchez, M. J. Rodríguez-Álvarez, J. P. Rigla, L. Moliner, A. Iborra, L. Hernández, D. Grau-Ruiz, A. J. González, J. J. García-Garrigos, E. Díaz-Caballero, P. Conde, A. Aguilar, L. Roso, and J. M. Benlloch, "Characterization of protons accelerated from a 3 TW table-top laser system .," *JINST*, 12 p. T05001, 2017.
- [5] R. F. W. A M Ghaderi, N P Ayerden, G de Graaf, "Minimizing stress in large-area surface micromachined perforated membranes with slits," *J. Micromechanics Microengineering*, vol. 25, p. 074010(9 p), 2015.
- [6] D. Jaeggi and B. Henry, "Thermal Converters by CMOS technology," PhD thesis, ETH Zurich, 1996.
- [7] F. Lindau, *Laser-driven particle acceleration*. Ph.D. thesis, Lund University, 2007.
- [8] S. Abedi, D. Dorranean, M. E. Abari, and B. Shokri, "Relativistic effects in the interaction of high intensity ultra-short laser pulse with collisional underdense plasma," *Phys. Plasmas*, vol. 18, no. 9, pp. 1–6, 2011.
- [9] M. Kaluza, J. Schreiber, M. I. K. Santala, G. D. Tsakiris, K. Eidmann, J. Meyer-Ter-Vehn, and K. J. Witte, "Influence of the laser prepulse on proton acceleration in thin-foil experiments," *Phys. Rev. Lett.*, 93 (4), 045003, 2004.
- [10] P. Antici, J. Fuchs, E. D'Humières, E. Lefebvre, M. Borghesi, E. Brambrink, C. A. Cecchetti, S. Gaillard, L. Romagnani, Y. Sentoku, T. Toncian, O. Willi, P. Audebert, and H. Pépin, "Energetic protons generated by ultrahigh contrast laser pulses interacting with ultrathin targets," *Phys. Plasmas*, vol. 14, no. 3, 2007.
- [11] T. Ceccotti, A. Lévy, H. Popescu, F. Réau, P. D'Oliveira, P. Monot, J. P. Geindre, E. Lefebvre, and P. Martin, "Proton acceleration with high-intensity ultrahigh-contrast laser pulses," *Phys. Rev. Lett.*, 99, 185002, 2007.
- [12] A. P. L. Robinson, P. Foster, D. Adams, D. C. Carroll, B. Dromey, S. Hawkes, S. Kar, Y. T. Li, K. Markey, P. McKenna, C. Spindloe, M. Streeter, C. G. Wahlström, M. H. Xu, M. Zepf, and D. Neely, "Spectral modification of laser-accelerated proton beams by self-generated magnetic fields," *New J. Phys.*, vol. 11, 2009.
- [13] M. Nishiuchi, H. Daido, A. Yogo, S. Orimo, K. Ogura, J. Ma, A. Sagisaka, M. Mori, A. S. Pirozhkov, H. Kiriya, S. V. Bulanov, T. Z. Esirkepov, I. W. Choi, C. M. Kim, T. M. Jeong, T. J. Yu, J. H. Sung, S. K. Lee, N. Hafz, K. H. Pae, Y. C. Noh, D. K. Ko, J. Lee, Y. Oishi, K. Nemoto, H. Nagatomo, K. Nagai, and H. Azuma, "Efficient production of a collimated MeV proton beam from a polyimide target driven by an intense femtosecond laser pulse," *Phys. Plasmas*, vol. 15, no. 5, 2008.
- [14] R. Zaffino, M. Seimetz, I. Sanchez, P. Mur, D. Quirion, P. Bellido, R. Lera, L. Martin, M. Lozano, and G. Pellegrini, "Efficient proton acceleration from a 3 TW table-top laser interacting with submicrometric mass-produced solid," *under Review*.